(Received 25 April 2024, Accepted 12 August 2024, Scheduled 24 August 2024)

A Planar Quad-Band Bandpass Filter Employing Transmission Lines Loaded with Tri-Stepped Impedance Open- and Dual-Stepped Impedance Short-Ended Resonators

Kamran Arif[1], Kanaparthi V. Phani Kumar [2,*], Rusan Kumar Barik [3], and Geetha Chakaravarthi[1]

[1]Department of Instrumentation and Control Engineering, National Institute of Technology Tiruchirappalli
Tiruchirappalli 620015, Tamil Nadu, India
[2]Department of Electronics and Communication Engineering, Faculty of Engineering and Technology
SRM Institute of Science and Technology, Kattankulathur-603203, Tamil Nadu, India
[3]School of Microelectronics, Southern University of Science and Technology, Shenzhen-518055, Guangdong, China

ABSTRACT: A highly miniaturized bandpass filter with quad-band response is demonstrated in this article. The proposed quad-band bandpass filter has a novel topology comprising series quarter wavelength transmission lines loaded with tri-stepped impedance open-ended resonators and a dual-stepped impedance short-ended resonator. The proposed quad-band bandpass filter configuration is validated by theoretically verifying the transmission zeros and pole frequencies using even-odd mode analysis. A prototype operating at 0.475 GHz, 1.695 GHz, 3.48 GHz, and 4.53 GHz is designed, implemented, and experimented. The tested insertion losses at these center frequencies are 0.38 dB, 0.71 dB, 1.03 dB, and 1.22 dB, and the return loss is better than 10 dB in each passband. Each passband is isolated by a transmission zero with a rejection better than 40 dB. The proposed quad-band filter occupies a compact size of $0.146 \times 0.087\lambda_g^2$ and is distinguished by its high compactness, wide bandwidth, multiple transmission zeros and poles, and high performance compared to benchmark designs making it more suitable for multi-band wireless applications.

1. INTRODUCTION

Radiofrequency/microwave multi-band band-pass filters (BPFs) have emerged as an essential component in radio frequency front-end systems within multi-standard wireless technologies. Multi-band bandpass filter with a smaller footprint area, multiple transmission zeros, high selectivity, low insertion loss, and cost-effectiveness has received a lot of attention in modern RF front-end systems. It is quite challenging for radio frequency (RF) researchers to develop multi-band bandpass filters that feature low attenuation, occupy a compact physical area, and possess a high level of selectivity in their passband. In recent years, several resonators have been exploited to implement multi-band bandpass filters [1–31]. In [1], a quad-band band-pass filter has been realized by using a metamaterial structure with an angular stub for Wi-Fi, WiMAX, ISM-band, and satellite applications. The suggested quad-band filter offers reflection coefficients of -26 dB, -40 dB, -23 dB, and -19 dB and insertion losses of 0.6 dB, 0.3 dB, 0.8 dB, and 0.3 dB at first, second, third, and fourth operating bands, respectively. In [2], a dual-mode dual square loop resonator (DMDSLR) has been proposed to realize a quad-band BPF. The DMDSLR resonator consists of meandered square loop resonators and stubbed T-couple lines. The resonant frequencies of the proposed quad-band BPF based on DMDSLR can be controlled by altering the parameters of the square loops.

Stepped Impedance Resonators (SIRs) of different configurations like asymmetric SIR [3], modified asymmetric SIR [4], and nested folded SIRs [5] have been used to realize quad-band BPFs. A quad-band BPF operating at GPS, WLAN, and WiMAX has been implemented by using a step impedance ring resonator (SIRR) [6]. To construct a directly coupled multi-band band-pass filter, a multi-stubs loaded ring resonator (MSLRR) topology has been proposed. Mixed electric and magnetic couplings have been employed in MSLRR to demonstrate the multi-mode resonant behavior [7]. The stub loaded resonators (SLRs) have been widely used in the design of quad-band band-pass filters. Inter-coupled quarter wavelength and half wavelength stub loaded resonators have been employed to demonstrate a quad-band BPF in [8]. In this design, the first and third passbands have been generated by a quarter wavelength resonator whereas the second and fourth passbands are produced by the half wavelength resonator. In [9], the quad-band BPF uses an open stub-loaded resonator (OSLR) and a short-stub-loaded resonator (SSLR). The OSLR and SSLR have been wrapped within one another, resulting in a small footprint, portable quad-band filter. The outer OSLR not only leads to the second and fourth bandpass but also feeds the SSLR. The inner SSLR leads to the first and third bandpasses. All bandpass frequencies can be controlled traditionally. In [10], an SLR along with a quarter wavelength res-

* Corresponding author: Kanaparthi V. Phani Kumar (kvphanikumar264@gmail.com).

onator has been utilized to realize a compact quad-band BPF. The proposed SLR not only creates lower passbands but also feeds the $\lambda/4$ resonator. In [11], a miniaturized quad-band BPF operating at 1.8 GHz, 2.45 GHz, 3.5 GHz, and 5.5 GHz has been realized for DCS, WLAN, WiMAX, and 5G applications. This quad-band BPF has been implemented using a multi-stub loaded resonator that exhibits first, second, and fourth passbands whereas the third passband is produced by a short-ended stub resonator. In [12], a miniaturized quad-band BPF has been constructed by using stub-loaded multi-mode resonators. This quad-band BPF operates at 0.94 GHz, 2.27 GHz, 3.55 GHz, and 5.66 GHz for GSM/LTE/WiMAX/WLAN applications. In [13], tri-/quad-/quint-/sext-/sept-band bandpass filters have been implemented by applying a low-pass filter and two short-ended stub-loaded resonators. These filters produce multiple transmission zeros along with several passbands which are controlled by the stub-load resonators. In [14], a quad-band BPF has been developed by combining two dual-band BPFs using an inter-digital capacitance-based common feed line. In this design, the dual-band BPFs have been realized by sung E-type stub-loaded resonators. The quad-band filter operates at 2.4 GHz, 3.5 GHz, 5.2 GHz, and 5.8 GHz with eight transmission zeros. In [15], dual-/tri-/quad-band BPFs have been developed by applying a three-section stepped impedance resonator having two-end shorted and two open stubs connected at the impedance junction. This quad-band BPF works at 1.19 GHz, 3.33 GHz, 5.87 GHz, and 8.39 GHz with insertion losses of 0.6 dB, 0.52 dB, 1.58 dB, and 1.3 dB. In [16], a QBBPF is realized using a dual-mode SLR and a sextuple mode resonator. The 1st, 2nd, and 4th passbands are generated using the proposed sextuple mode resonator, and the 3rd passband is obtained due to dual-mode SLR.

Two distinct dual-band BPFs, one realized using parallel coupled lines and lumped inductors and the other based on the half wave and quarter wavelength SIRs, are combined to implement a quad-band BPF [17]. A narrowband QBBPF with fractional bandwidths 5.3%, 5.5%, 3.2%, and 3.6% is realized using coupled lines connected to a semi-circular resonator loaded with open stubs [18]. The suggested quad-band filter operates at 1.55 GHz, 2.79 GHz, 3.29 GHz, and 4.47 GHz along with nine transmission zeros. In [19], a miniaturized quad-band BPF has been developed by employing multiple coupling networks and quad-mode stepped impedance resonators (QMSIRs). In this design, even- and odd-mode analysis has been applied to the analytical derivation of design equations. The suggested quad-band filter works at 2.59 GHz, 3.46 GHz, 5.33 GHz, and 6.65 GHz along with nine transmission zeros. However, the quad-band filter suffers from large insertion losses of 1.9 dB, 1.6 dB, 3.5 dB, and 3.2 dB. In [20], the generation of multiband band-pass filters (MBPFs) having an inline structure has been described. The multi-channel characteristics and smaller footprint area have been realized by applying multi-coupled structures. The proposed quad-band BPF operates at 0.8 GHz, 3.25 GHz, 3.54 GHz, and 3.755 GHz with 3-dB fractional bandwidths of 3.33%, 2.25%, 3.25%, and 2.93%, respectively but produces larger insertion losses of 1.56 dB, 2.38 dB, 1.61 dB, and 1.28 dB. In [21], a quad-band high-temperature super-conducting BPF has been realized by employing stepped impedance resonators. This quad-band filter offers 3-dB fractional bandwidths of 4.8%, 3.96%, 3.97%, and 2.2% at the center frequencies of 1.2 GHz, 2.52 GHz, 3.51 GHz, and 4.44 GHz, respectively. In [22], a quad-band BPF has been created by using screen printing technology for GSM, WiMAX, and WLAN applications. This quad-band filter has been realized on a ceramic substrate which consists of a U-shaped resonator, defected ground structures, and an end-coupled transmission line. The suggested filter provides 3-dB fractional bandwidths of 9.55%, 31.8%, 11.1%, and 15.9% at 1.57 GHz, 2.45 GHz, 3.5 GHz, and 5.2 GHz, respectively.

A miniaturized quad-band BPF has been designed by applying a quintuple-mode resonator for GPS/WLAN/WiMAX/5G applications [23]. In [24], a quad-mode resonator-based bandpass filter has been realized utilizing a half-mode substrate-integrated waveguide. In [25], an ultra-compact bandpass filter has been developed based on a half-mode substrate integrated rectangular resonator for wide passband and low insertion loss. In [26], an order extensible substrate-integrated waveguide based band-pass filter has been constructed that exhibits broadband response and low insertion. In [27], a quad-mode defected ground structure has been employed for the realization of a quad-mode BPF. In [28], a modified coaxial cavity resonator has been applied to the implementation of a quad-mode BPF. In [29], a miniaturized quad-band BPF has been constructed by using a multi-layered structure that connects the impedances inductively with stepped impedance resonators. This quad-band filter achieves low insertion losses of 0.2 dB, 0.3 dB, 0.3 dB, and 0.4 dB, at the operating frequencies of 1.57 GHz, 2.4 GHz, 3.5 GHz, and 5.2 GHz, respectively. In [30], four transmission lines formed in a square ring are placed in between two series microstrip lines to realize a quad-band high-temperature super-conducting BPF. The suggested quad-band filter exhibits 3-dB fractional bandwidths of 4.96%, 5.07%, 2.32%, and 3.63%, and insertion losses of 0.12 dB, 0.12 dB, 0.23 dB, and 0.25 dB at the center frequencies of 2.45 GHz, 3.55 GHz, 5.18 GHz, and 5.79 GHz, respectively. In [31], two sets of different stepped impedance resonators have been employed for the development of a quad-band BPF. This quad-band filter has center frequencies of 2.0 GH, 3.0 GHz, 3.9 GHz, and 7.2 GHz, insertion losses of 1.1, 1.9, 1.0, and 2.1, and 3-dB fractional bandwidths of 14/6.7/13.3/2.6-percent. The design of a quad-band BPF with a small footprint, low insertion loss, good selectivity, and multiple transmission zeros remains a tough challenge, despite the impressive performances of the previously stated filters.

In this paper, a novel topology comprising series quarter wavelength transformers loaded with tri-stepped impedance open-ended resonators and a dual-stepped impedance short-ended resonator is proposed to realize a highly compact band-pass filter with quad-band response. A couple of quarter wavelength transformers loaded with a dual-stepped impedance short-ended resonator at the centre provide two wide passbands. The two wide passbands are truncated into four by the tri-stepped impedance open-ended resonators included at the input and output sides. Based on this novel topology, a quad-band band-pass filter with specifications of 0.475 GHz, 1.695 GHz, 3.48 GHz, and 4.53 GHz, and 3 dB fractional bandwidths of 124.21%, 54.86%, 25.86%, and 7.94%, respectively, is de-

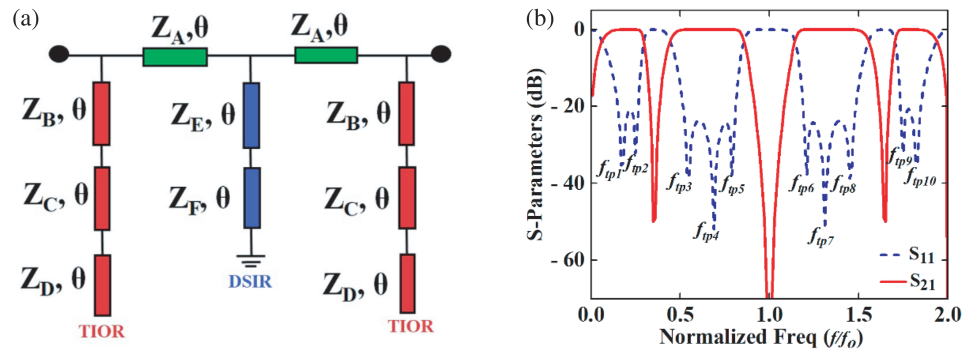

FIGURE 1. Schematic of the proposed quad-band BPF using QWTs loaded with TIOR and DSIR units. (a) Transmission line configuration and (b) circuit simulated frequency response. Units: Ω, $Z_A = 62$, $Z_B = 75$, $Z_C = 120$, $Z_D = 100$, $Z_E = 80$, $Z_F = 140$.

signed. The frequencies of the five transmission zeros in the stopband and ten transmission poles in the passbands are verified using the even-odd mode analysis. Analysis of the four passbands with respect to the impedances of the proposed configuration is presented. The passband bandwidths can be controlled simultaneously by changing the impedances of the filter configuration. A full-wave electromagnetic simulator is used to build and model the proposed quad-band circuit. Keysight vector network analyser is utilized to measure the manufactured circuit. The outcomes are then quantitatively contrasted with the other results that have been published in the references. Eventually, a quantitative comparison is made between the obtained results and the other reported results in the references. The highlights of the proposed quad-band filter are

i The passbands have wide 3 dB fractional bandwidths (124.21%, 54.86%, 25.86%, and 7.94%).

ii High isolation between the passbands with a rejection better than 40 dB.

iii A compact circuit size of $0.146 \times 0.087\ \lambda_g^2$.

iv Multiple transmission zeros and poles indicate high selectivity.

2. DESIGN AND ANALYSIS OF THE PROPOSED QUAD-BAND BPF

The transmission line configuration and circuit simulated frequency responses of the proposed quad-band BPF are illustrated in Figs. 1(a) and 1(b), respectively. The proposed quad-band BPF transmission line model consists of series quarter wave transformers (Z_A, θ), loaded with tri-stepped impedance open-ended resonators (Z_B, θ), (Z_C, θ) & (Z_D, θ), and a dual-stepped impedance short-ended resonator (Z_E, θ) & (Z_F, θ). The ideal circuit simulated frequency response contains four passbands out of which two passbands contain two poles each, and the other two passbands contain three poles each. The frequency response also contains a total of five transmission zeros in the stopband. Initially, a dual-stepped impedance short-ended resonator (DSIR) loaded at the center of the two quarter wavelength transformers (QWTs) is simulated, and the frequency response is depicted in Fig. 2. The response contains three transmission zeros f_{tz1}, f_{tz3}, f_{tz5} at 0, f_0, $2f_0$, respectively. Next, the DSIR is removed, and the series QWTs

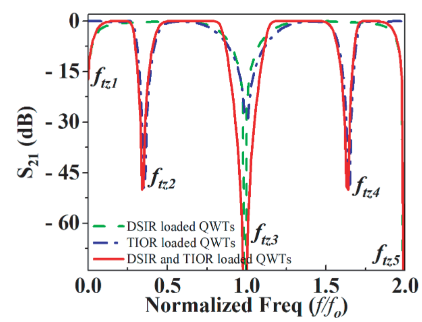

FIGURE 2. Circuit simulated frequency response (S_{21}) for the QWTs loaded with DSIR and TIOR.

are loaded with tri-stepped impedance open-ended resonators (TIORs) at the input and output ports. The frequency response of QWTs loaded with TIORs contains three transmission zeros f_{tz2}, f_{tz3}, and f_{tz4}, as shown in Fig. 2. In the last stage of circuit analysis, the QWTs are loaded with both DSIR and TIORs and is simulated in a circuit simulator. The transmission zeros generated due to QWTs loaded with DSIR and TIOR are overlapped, and a quad-band band-pass response is achieved. Each passband is separated by a transmission zero with a rejection better than 40 dB. At f_0 there are two transmission zeros, one due to DSIR and the other due to TIOR. To validate the proposed filter configuration and its frequency response, theoretical analysis based on even and odd mode techniques is employed. Figs. 3(a) and 3(b) depict the even and odd mode transmission line equivalent circuits of the proposed quad-band BPF using QWTs loaded with TIOR and DSIR units.

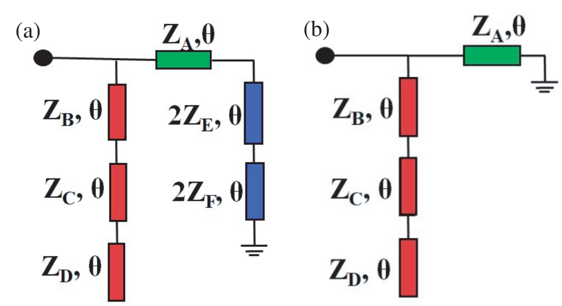

FIGURE 3. The proposed quad-band BPF using QWTs loaded with TIOR and DSIR units (a) even (b) odd mode transmission line models.

From the lossless transmission line theory, the input impedances Z_{inE} and Z_{inO} of the even and odd mode circuits, respectively, can be written as

$$Z_{inE} = \frac{Z_{S1}Z_{SE2}}{Z_{S1}+Z_{SE2}} \tag{1}$$

$$Z_{inO} = \frac{Z_{S1}Z_{SO2}}{Z_{S1}+Z_{SO2}} \tag{2}$$

where

$$Z_{S1} = j\left[\frac{N_{1S}+N_{2S}\tan^2\theta}{D_{1S}\tan\theta+D_{2S}\tan^3\theta}\right] \tag{3a}$$

$$Z_{SE2} = j\left[\frac{N_{1E}\tan\theta+N_{2E}\tan^3\theta}{D_{1E}+D_{2E}\tan^2\theta}\right] \tag{3b}$$

$$Z_{SO2} = jZ_A\tan\theta \tag{3c}$$

$$N_{1S} = -Z_BZ_CZ_D \tag{3d}$$

$$N_{2S} = Z_BZ_C^2+Z_B^2(Z_C+Z_D) \tag{3e}$$

$$D_{1S} = Z_BZ_C+Z_BZ_D+Z_CZ_D \tag{3f}$$

$$D_{2S} = -Z_C^2 \tag{3g}$$

$$N_{1E} = 2Z_AZ_E^2+2Z_AZ_EZ_F+2Z_A^2Z_E^2 \tag{3h}$$

$$N_{2E} = -Z_A^2Z_F \tag{3i}$$

$$D_{1E} = Z_AZ_E \tag{3j}$$

$$D_{2E} = -(Z_AZ_F+2Z_E^2+2Z_EZ_F) \tag{3k}$$

From (1) and (2), the input admittances (Y_{inE} and Y_{inO}) can be obtained. The S-parameters of the overall filter unit can be written as [32]

$$S_{11} = \frac{Y_o^2-Y_{inE}Y_{inO}}{(Y_o^2+Y_{inE})(Y_o^2+Y_{inO})} \tag{4}$$

$$S_{21} = \frac{Y_o(Y_{inE}-Y_{inO})}{(Y_o^2+Y_{inE})(Y_o^2+Y_{inO})} \tag{5}$$

The transmission zero frequencies (f_{TZ}) of the proposed QBBPF using QWTs loaded with TIOR and DSIR units can be obtained by setting $|S_{21}|=0$. Replacing θ by θ_{TZ} and simplifying the equation $|S_{21}|=0$, we get two equations

$$(Z_BZ_C^2+Z_B^2Z_C+Z_B^2Z_D)\tan^2\theta_{TZ}-Z_BZ_CZ_D = 0 \tag{6}$$

$$2Z_E(Z_E+Z_F)\tan\theta_{TZ}\left[\tan^2\theta_{TZ}+1\right] = 0 \tag{7}$$

From (6) and (7), θ_{TZ} can be solved, and then the transmission zero frequencies of the proposed QBBPF can be computed from (8)–(12).

$$f_{tz1} = 0 \tag{8}$$

$$f_{tz2} = \frac{f_0}{\theta_0}\arctan\sqrt{\frac{Z_BZ_CZ_D}{Z_BZ_C^2+Z_B^2Z_C+Z_B^2Z_D}} \tag{9}$$

$$f_{tz3} = f_0 \tag{10}$$

$$f_{tz4} = 2f_0-f_{tz2} \tag{11}$$

$$f_{tz5} = 2f_0 \tag{12}$$

Similarly, the transmission poles of the proposed quad-band BPF using QWTs loaded with TIOR and DSIR units can be found by setting $|S_{11}|=0$. Replacing θ by θ_{TP} and simplifying $|S_{11}|=0$, we get

$$K_1(\tan^2\theta_{TP})^5+K_2(\tan^2\theta_{TP})^4+K_3(\tan^2\theta_{TP})^3 +K_4(\tan^2\theta_{TP})^2+K_5\tan^2\theta_{TP}+K_6=0 \tag{13}$$

where

$$K_1 = A \tag{13a}$$

$$K_2 = B+Y_0^2G \tag{13b}$$

$$K_3 = C+Y_0^2H \tag{13c}$$

$$K_5 = E+Y_0^2J \tag{13d}$$

$$K_6 = F \tag{13e}$$

$$A = D_{2S}Z_AV \tag{14a}$$

$$B = D_{2S}Z_AU+(N_{2S}+D_{1S}Z_A)V \tag{14b}$$

$$C = D_{2S}Z_AT+(N_{2S}+D_{1S}Z_A)U+N_{1S}V \tag{14c}$$

$$D = D_{2S}Z_AS+(N_{2S}+D_{1S}Z_A)T+N_{1S}U \tag{14d}$$

$$E = (N_{2S}+D_{1S}Z_A)S+N_{1S}T \tag{14e}$$

$$F = N_{1S}S \tag{14f}$$

$$G = N_{2S}Z_AR \tag{14g}$$

$$H = N_{2S}Z_AQ+N_{1S}Z_AR \tag{14h}$$

$$I = N_{2S}Z_AP+N_{1S}Z_AQ \tag{14i}$$

$$J = N_{1S}Z_AP \tag{14j}$$

$$P = N_{1S}N_{1E} \tag{15a}$$

$$Q = N_{1S}N_{2E}+N_{2S}N_{1E} \tag{15b}$$

$$R = N_{2S}N_{2E} \tag{15c}$$

$$S = N_{1S}D_{1E} \tag{15d}$$

$$T = N_{1S}D_{2E}+N_{2S}D_{1E}+N_{1E}D_{1S} \tag{15e}$$

$$U = N_{2S}D_{2E}+N_{1E}D_{2S}+N_{2E}D_{1S} \tag{15f}$$

$$V = N_{2E}D_{2S} \tag{15g}$$

By solving (13) using any math tool, we get ten real solutions for θ_{TP}. Therefore, the transmission pole frequencies f_{TPn} can be determined using (16)

$$f_{TPn} = \frac{\theta_{TPn}}{\theta_o}f_0, \quad n=1,2,\ldots,10 \tag{16}$$

Table 1 shows the theoretically calculated and simulated transmission zeros and pole frequencies for a typical example. They are identical, validating the proposed quad-band BPF configuration and theory.

Figure 4 shows the S-parameter variations of the proposed quad-band BPF for changes in impedance parameters (Z_A, Z_B, Z_C, Z_D, Z_E, & Z_F). The return loss in all four passbands increases as the impedance Z_A increases, as shown in Fig. 4(a). When Z_B, Z_C, and Z_E increase, there is no significant variation in the first and fourth passband; however, the return loss in the second and third passband changes, as illustrated in Figs. 4(b), (c), and (e), respectively. There is a shift in the second and fourth transmission zero frequencies when there is a change in the impedance Z_D, as shown in Fig. 4(d). When Z_F

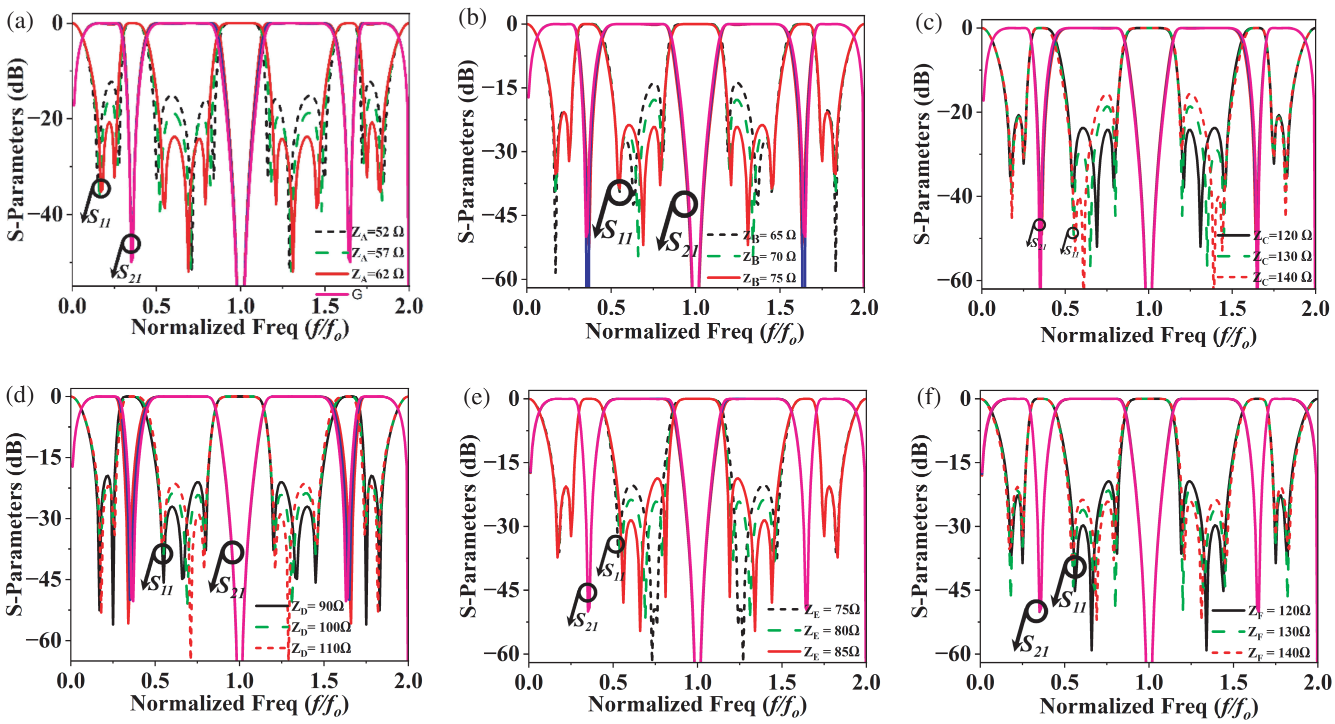

FIGURE 4. S-parameter variations with changes in (a) Z_A, (b) Z_B, (c) Z_C, (d) Z_D, (e) Z_E, and (f) Z_F.

TABLE 1. Theoretical and circuit-simulated Transmission Zeros and poles frequencies (Units: Ω, $Z_A = 62$, $Z_B = 75$, $Z_C = 120$, $Z_D = 100$, $Z_E = 80$, $Z_F = 140$).

Transmission zeros (GHz)		
Frequencies	Theoretical	Circuit simulated
f_{tz1}	0	0
f_{tz2}	0.35	0.35
f_{tz3}	1.0	1.0
f_{tz4}	1.65	1.65
f_{tz5}	2.0	2.0
Transmission poles (GHz)		
f_{tp1}	0.17	0.17
f_{tp2}	0.25	0.25
f_{tp3}	0.55	0.55
f_{tp4}	0.69	0.69
f_{tp5}	0.79	0.79
f_{tp6}	1.21	1.21
f_{tp7}	1.31	1.31
f_{tp8}	1.45	1.45
f_{tp9}	1.75	1.75
f_{tp10}	1.83	1.83

increases, the return loss in all four passbands decreases, and there is no change in the transmission zero frequencies. This parametric study helps the designer to select the required return loss level in the passbands and also the transmission zero and pole positions.

3. IMPLEMENTATION AND RESULTS

The circuit parameters of the proposed quad-band BPF using QWTs loaded with TIOR and DSIR units are finalized based on the design flowchart illustrated in Fig. 5. The parameter values considered for prototype implementation are $Z_A = 62\,\Omega$, $Z_B = 75\,\Omega$, $Z_C = 120\,\Omega$, $Z_D = 100\,\Omega$, $Z_E = 80\,\Omega$, $Z_F = 140\,\Omega$, $f_0 = 2.7\,\text{GHz}$. The proposed quad-band BPF is designed on a Rogers RT Duroid 5880 substrate ($\varepsilon_r = 2.2$,

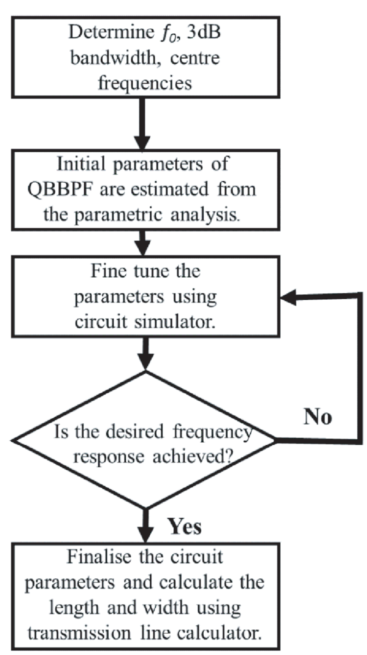

FIGURE 5. Design flowchart of the proposed quad-band BPF.

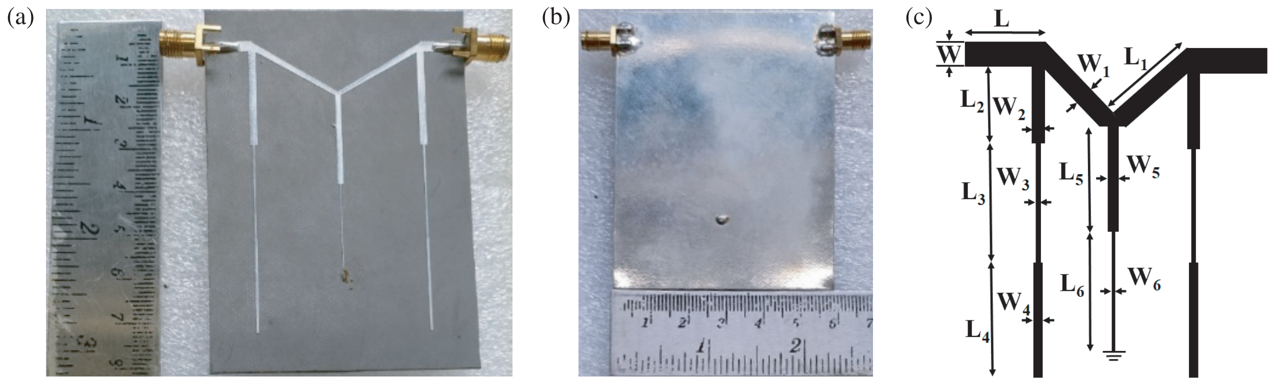

FIGURE 6. Fabricated prototype of the proposed quad-band BPF using QWTs loaded with TIOR and DSIR units (a) top view, (b) bottom view and (c) layout.

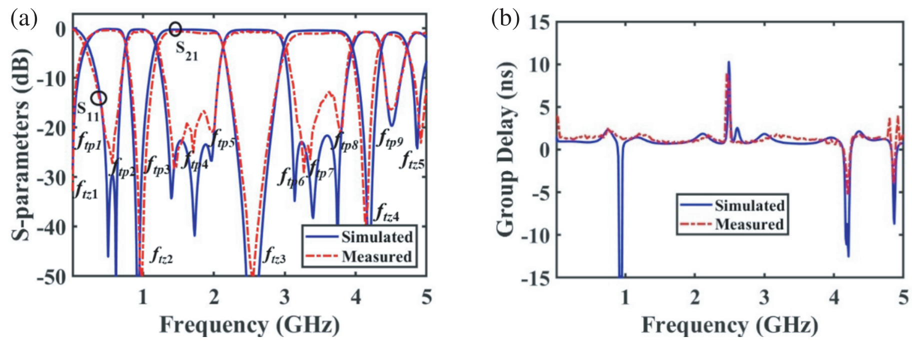

FIGURE 7. Simulated and measured (a) S_{11}, S_{21} and (b) group delay of the quad-band BPF based on QWTs loaded with TIOR and DSIR units.

TABLE 2. Simulated and measured results of the proposed quad-band BPF using QWTs loaded with TIOR and DSIR units.

Parameter	First Passband		Second Passband		Third Passbnad		Fourth Passband	
	Sim.	Meas.	Sim.	Meas.	Sim.	Meas.	Sim.	Meas.
f_C (GHz)	0.485	0.475	1.655	1.695	3.47	3.48	4.545	4.53
IL (dB)	0.31	0.38	0.33	0.71	0.33	1.03	0.46	1.22
RL (dB)	29.33	22.34	22.90	20.65	21.60	16.65	19.67	16.10
3 dB Bandwidth (GHz)	0.55	0.59	0.95	0.93	0.98	0.90	0.37	0.36
3 dB FBW (%)	113.40	124.21	57.40	54.86	28.24	25.86	8.14	7.94
Roll-off rate (dB/GHz)	73.91/170	100/141.67	94.44/130.77	100/94.45	141.67/100	70.84/106.25	113.33/77.28	121.42/77.28

loss tangent $= 0.0012$, and $h = 0.79$ mm) and simulated in ANSYS High-Frequency Structure Simulator. The fabricated quad-band BPF prototype and its layout are depicted in Figs. 6(a), (b), and (c), respectively. The physical dimensions (in mm) of the fabricated filter are summarized as follows: $L = 10$, $L_1 = 23.67$, $L_2 = 21.87$, $L_3 = 21.33$, $L_4 = 21.06$, $L_5 = 20.75$, $L_6 = 21.39$, $W = 2.38$, $W_1 = 1.81$, $W_2 = 1.68$, $W_3 = 0.4$, $W_4 = 0.65$, $W_5 = 1.31$, $W_6 = 0.25$ (dimensions in mm). The overall size of the fabricated quad-band BPF using TIOR and DSIR is $0.146\lambda_g \times 0.087\lambda_g$, where λ_g is the guided wavelength at the first center frequency. The measured results of the proposed quad-band BPF using QWTs loaded with TIOR and DSIR units are characterized in a Keysight vector network analyzer. The simulated and experimented S_{11} and S_{21} are compared and illustrated in Figs. 7(a)–(b). The fabricated quad-band BPF has measured passband center frequencies at 0.475, 1.695, 3.48, and 4.53 GHz, and the corresponding 3-dB fractional bandwidths (FBWs) are 124.21%, 54.86%, 25.86%, and 7.94%, respectively. The measured minimum insertion losses in the four passbands are 0.38 dB, 0.71 dB, 1.03 dB, and 1.22 dB. The tested return loss is better than 20 dB in all the passbands. The simulated and experimented group delays are

TABLE 3. Performance comparison with previously reported quad-band BPFs.

Ref.	f_c (GHz)	TZs/TPs	RL (dB)	IL (dB)	3 dB FBW (%)	Circuit Size $(\lambda_g \times \lambda_g)/\lambda_g^2$
[2]	2.40, 3.59, 5.22, 6.60	8/8	30, 10, 17, 10.5	0.72, 0.68, 1.30, 1.39	12, 10.70, 8.54, 5.03	—
[3]	2.4, 3.5, 5.2, 6.8	-/-	13, 38, 19, 26	0.5, 1.3, 1.3, 1	6.4, 9.4, 3.8, 4.9	0.3 × 0.3
[4]	2.35, 3.80, 5.20, 6.55	6/8	21, 18, 17, 23	0.90, 1.20, 1.35, 1.50	7.2, 4.1, 3.6, 2.7	0.38 × 0.15
[6]	1.57, 2.45, 3.50, 5.20	5/4	—	0.78, 1.45, 2.30, 1.42	6.9, 3.4, 2.9, 4.7	0.2 × 0.3
[7]	1.91, 3.55, 5.36, 6.92	4/6	—	0.60, 1.65, 1.05, 1.85	16.5, 6.9, 7.4, 5.4	0.232 × 0.121
[8]	2.4, 3.5, 5.2, 6.8	5/4	32, 29, 25, 29	0.70, 0.74, 1.1, 1.2	—	0.25 × 0.30
[9]	1.32, 1.71, 2.41, 3.41	6/7	18, 21, 24, 22	1.1, 1.3, 0.5, 0.5	9.1, 5.8, 15.7, 11.4	0.21 × 0.22
[13]	0.96, 2.51, 3.71, 5.11	5/7	—	0.12, 0.70, 0.30, 0.53	109.40, 30.40, 20.8, 35.20	0.14 × 0.14
[14]	2.4, 3.5, 5.2, 5.8	8/8	15.5, 14.5, 21, 16	2, 1.90, 1.90, 1.96	6.7, 7.2, 6.9, 5.3	0.16 × 0.25
[16]	1.75, 2.45, 3.50, 5.25	4/8	14.80, 15.70, 12.18, 12.80	1.06, 0.89, 1.54, 1.10	5.7, 4.1, 5.7, 3.8	0.13 × 0.22
[17]	1.55, 2.79, 3.29, 4.47	7/5	12.2, 13.64, 13.98, 14.5	3.63, 2.51, 2.89, 4.48	3.10, 3.22, 2.79,2.23	0.26 × 0.076
[18]	2.62, 2.88, 4.34 4.67	4/4	18.5, 15.51, 20, 17.5	0.97, 0.86, 1.37, 1.09	5.3, 5.5, 3.2, 3.6	0.079
[19]	2.40, 3.30, 5.38, 6.48	5/9	14, 21.8, 16, 11.3	1.9, 1.6, 3.5, 3.2	3.0, 6.41, 3.70, 4.56	0.28 × 0.18
[20]	0.8, 3.25, 3.54, 3.755	—	10.8, 13.9, 14.5, 12.9	1.56, 2.38, 1.63, 1.28	3.33, 2.25, 3.25, 2.93	0.11 × 0.11
[22]	1.57, 2.45, 3.50, 5.20	4/8	—	0.31, 0.32, 0.31, 0.78	9.55, 31.80, 11.10, 15.90	—
[23]	1.55, 4.06, 2.46, 5.08	4/8	12.2, 13.64, 13.98, 14.5	1.95, 1.61, 1.17, 1.55	9.55, 31.80, 11.10, 15.90	0.024 × 0.024
[31]	2.0, 3.0, 3.9, 7.2	6/6	20.77, 20.68, 23.34, 28.46	1.1, 1.9, 1.0, 2.1	14, 6.7, 113.3, 26	0.11 × 0.38
This work	**0.47, 1.69, 3.48, 4.53**	**5/9**	**29.85, 22.60, 21.62, 19.67**	**0.38, 0.71, 1.03, 1.22**	**124.21, 54.86, 25.86, 7.94**	**0.146 × 0.087**

depicted in Fig. 7(b). The group delay variations are 1.26–1.66 ns, 0.76–1.71 ns, 0.74–1.8 ns, and 1.25–1.75 ns in the 1st, 2nd, 3rd, and 4th passbands, respectively. Table 2 shows the comparison between the simulated and measured results of the proposed quad-band BPF. The experimented data is in good agreement with the simulated one.

Table 3 presents a performance comparison of the quad-band BPF using QWTs loaded with TIOR and DSIR units with some previously reported works. The proposed quad-band BPF exhibits a compact size of $0.146\lambda_g \times 0.087\lambda_g$ compared to all the state-of-the-art designs. The proposed filter realizes nine transmission poles that are high compared to other benchmark quad-band BPFs. Overall, the proposed quad-band BPF using a novel combination of series QWTs, DSIR, and TIORs has superior performances in almost all aspects when being matched to the reported quad-band BPFs.

4. CONCLUSION

A novel topology composed of series quarter wavelength transformers loaded with a dual-stepped impedance resonator at the center and tri-stepped impedance resonators at the input and output sides is proposed in this work to realize a band-pass filter with a quad-band response. The frequency locations of five transmission zeros and ten transmission poles obtained from the ideal circuit simulator are verified theoretically using even-odd mode analysis. The developed quad-band band-pass filter has center frequencies at 0.475, 1.695, 3.48, 4.53 GHz, and the corresponding 3-dB fractional bandwidths are 124.21%, 54.86%, 25.86%, and 7.94%, respectively. The experimental results of the quad-band filter using QWTs loaded with TIOR and DSIR units provide strong support for theoretical predictions. The suggested quad-band filter has many appealing qualities that make it a good fit for use in a multimode modern communication system, including its compact size, wide passbands, high isolation, and selectivity.

REFERENCES

[1] Bashir, G. and T. Shanmuganantham, "Design of metamaterial quad-band bandpass filter," in *2019 International Conference on Wireless Communications Signal Processing and Networking (WiSPNET)*, 324–327, Chennai, India, 2019.

[2] Liu, J.-C., F. S. Huang, and C.-P. Kuei, "Quad-band dual-mode resonator with dual-square-loop for WLAN and WiMAX systems," in *CSQRWC 2012*, 100–103, New Taipei, Taiwan, 2012.

[3] Wu, H.-W. and R.-Y. Yang, "A new quad-band bandpass filter using asymmetric stepped impedance resonators," *IEEE Microwave and Wireless Components Letters*, Vol. 21, No. 4, 203–205, 2011.

[4] Chen, S.-P., Y.-W. Chen, S.-P. Wu, H.-W. Wu, and C.-Y.-D. Sim, "Quad-band bandpass filter using modified asymmetric stepped impedance resonators," in *2021 51st European Microwave Conference (EuMC)*, 305–308, London, United Kingdom, 2022.

[5] Long, X.-Y., W. Shen, M.-Q. Li, Y. Zhu, Y.-D. Wei, and Y. Hou, "A novel quad-band filter with high skirt selectivity using nested folded SIRs," in *2016 IEEE International Conference on Microwave and Millimeter Wave Technology (ICMMT)*, Vol. 1, 302–305, Beijing, China, 2016.

[6] Wei, F., Q. Huang, X. H. Wang, W.-T. Li, and X.-W. Shi, "Compact step-impedance ring resonator for quad-band band-pass filter," *Progress In Electromagnetics Research Letters*, Vol. 41, 105–112, 2013.

[7] Xu, J., W. Wu, and G. Wei, "Compact multi-band bandpass filters with mixed electric and magnetic coupling using multiple-mode resonator," *IEEE Transactions on Microwave Theory and Techniques*, Vol. 63, No. 12, 3909–3919, 2015.

[8] Virdee, B. S., M. Farhat, and M. Riaz, "Compact quad-band bandpass filter based on stub-loaded resonators," in *2017 IEEE MTT-S International Microwave Symposium (IMS)*, 1927–1929, Honololu, HI, USA, 2017.

[9] Zhu, H., L. Gao, X. Y. Zhang, and B.-J. Hu, "Design of quad-band bandpass filter using open-and short-stub-loaded resonators," in *Proceedings of 2011 Cross Strait Quad-Regional Radio Science and Wireless Technology Conference*, Vol. 1, 661–663, Harbin, China, 2011.

[10] Ma, Y., B. Liu, Z. Guo, R. Zhao, X. Wei, W. Xing, and Y. Wang, "A compact quad-band bandpass filter with high skirt selectivity based on stub-loaded resonators and $\lambda/4$ resonators," in *2018 IEEE MTT-S International Wireless Symposium (IWS)*, 1–4, Harbin, China, 2018.

[11] Zhang, Y., L. Gao, and X. Y. Zhang, "Compact quad-band bandpass filter for DCS/WLAN/WiMAX/5G Wi-Fi application," *IEEE Microwave and Wireless Components Letters*, Vol. 25, No. 10, 645–647, 2015.

[12] Murmu, L. and S. Das, "A compact quad-band bandpass filter using multi-mode stub-loaded resonator," *Progress In Electromagnetics Research Letters*, Vol. 61, 39–46, 2016.

[13] Yang, Q., Y.-C. Jiao, and Z. Zhang, "Compact multiband bandpass filter using low-pass filter combined with open stub-loaded shorted stub," *IEEE Transactions on Microwave Theory and Techniques*, Vol. 66, No. 4, 1926–1938, 2018.

[14] Yan, T., X.-H. Tang, and J. Wang, "A novel quad-band bandpass filter using short stub loaded E-shaped resonators," *IEEE Microwave and Wireless Components Letters*, Vol. 25, No. 8, 508–510, 2015.

[15] Xu, J., W. Wu, and C. Miao, "Compact microstrip dual-/tri-/quad-band bandpass filter using open stubs loaded shorted stepped-impedance resonator," *IEEE Transactions on Microwave Theory and Techniques*, Vol. 61, No. 9, 3187–3199, 2013.

[16] Tantiviwat, S., S. Z. Ibrahim, M. S. Razalli, and S. P. Jack, "Quad-band bandpass filter based on sextuple-mode and dual-mode stub-loaded resonators," *AEU — International Journal of Electronics and Communications*, Vol. 111, 152914, 2019.

[17] Lin, S.-C., "Microstrip dual/quad-band filters with coupled lines and quasi-lumped impedance inverters based on parallel-path transmission," *IEEE Transactions on Microwave Theory and Techniques*, Vol. 59, No. 8, 1937–1946, 2011.

[18] Noori, L. and A. Rezaei, "Design of microstrip wide stopband quad-band bandpass filters for multi-service communication systems," *AEU — International Journal of Electronics and Communications*, Vol. 81, 136–142, 2017.

[19] Bukuru, D., K. Song, F. Zhang, Y. Zhu, and M. Fan, "Compact quad-band bandpass filter using quad-mode stepped impedance resonator and multiple coupling circuits," *IEEE Transactions on Microwave Theory and Techniques*, Vol. 65, No. 3, 783–791, 2017.

[20] Wu, Y. and K. Ma, "Design of multiband bandpass inline topology filters using compact multicoupled line structures," *IEEE Transactions on Components, Packaging and Manufacturing Technology*, Vol. 13, No. 3, 382–390, 2023.

[21] Zhang, J., Q. Liu, D.-W. Zhang, and Y. Qu, "High selectivity single wideband and quad-band HTS filters using novel quad-mode resonators with self-coupled structure," *IEEE Access*, Vol. 9, 103 194–103 203, 2021.

[22] Cheng, C.-M. and C.-F. Yang, "Develop quad-band (1.57/2.45/3.5/5.2 GHz) bandpass filters on the ceramic substrate," *IEEE Microwave and Wireless Components Letters*, Vol. 20, No. 5, 268–270, 2010.

[23] Mirzaei, M. and M. A. Honarvar, "Compact planar quad-band bandpass filter for application in GPS, WLAN, WiMAX and 5G WiFi," *Progress In Electromagnetics Research Letters*, Vol. 63, 115–121, 2016.

[24] Wu, X., W.-J. Wu, Y. Cao, and G. Wang, "Novel compact half-mode SIW bandpass filters based on quad-mode resonator," *IEEE Transactions on Circuits and Systems II: Express Briefs*, Vol. 70, No. 1, 96–100, 2022.

[25] Barik, R. K., S. Koziel, and A. Pietrenko-Dabrowska, "Broad stopband, low-loss, and ultra-compact dual-mode bandpass filter based on HMSIRC," *Electronics*, Vol. 12, No. 13, 2831, 2023.

[26] Barik, R. K. and S. Koziel, "Compact, order extensible and wide-stopband bandpass filter based on SIW cavity with rectangular ring slot," *IEEE Transactions on Circuits and Systems II: Express Briefs*, Vol. 69, No. 12, 4784–4788, 2022.

[27] Peng, B., S. Li, J. Zhu, Q. Zhang, L. Deng, Q. Zeng, and Y. Gao, "Compact quad-mode bandpass filter based on quad-mode DGS resonator," *IEEE Microwave and Wireless Components Letters*, Vol. 26, No. 4, 234–236, 2016.

[28] Wang, X., G. Jang, B. Lee, and N. Park, "Compact quad-mode bandpass filter using modified coaxial cavity resonator with improved Q-factor," *IEEE Transactions on Microwave Theory and Techniques*, Vol. 63, No. 3, 965–975, 2015.

[29] Wu, H.-W. and C.-T. Chiu, "Design of compact multi-layered quad-band bandpass filter," *IEEE Microwave and Wireless Components Letters*, Vol. 26, No. 11, 879–881, 2016.

[30] Liu, H., B. Ren, X. Guan, P. Wen, and Y. Wang, "Quad-band high-temperature superconducting bandpass filter using quadruple-mode square ring loaded resonator," *IEEE Transactions on Microwave Theory and Techniques*, Vol. 62, No. 12, 2931–2941, 2014.

[31] Da Xu, K. and J. Ai, "Compact microstrip quad-band bandpass filter using stub-loaded SIRs," in *2015 Asia-Pacific Microwave Conference (APMC)*, Vol. 3, 1–3, Nanjing, China, 2015.

[32] Alazemi, A. J., "A compact diamond-shaped dual-band bandpass filter with multiple transmission zeros," *AEU — International Journal of Electronics and Communications*, Vol. 162, 154591, 2023.